ChemComm

COMMUNICATION

View Article Online
View Journal | View Issue

Cite this: *Chem. Commun.*, 2023, 59, 10307

Received 27th May 2023,
Accepted 31st July 2023

DOI: 10.1039/d3cc02560h

rsc.li/chemcomm

Extending Se substitution to the limit: from 5S to 5Se in high-efficiency non-fullerene acceptors†

Guangkun Song,‡[a] Wanying Feng,‡[a] Yu Li,[a] Huazhe Liang,[a] Zhixiang Li,[a] Bin Kan,[b] Xiangjian Wan,[a] Zhaoyang Yao,*[a] Chenxi Li[a] and Yongsheng Chen*[a]

Based on the newly synthesized seleno[3,2-*b*]selenophene unit, two near-infrared non-fullerene acceptors (NFAs) of 4Se and 5Se are constructed by replacing four or all sulfurs with selenium in high-efficiency Y-series NFAs. Consequently, binary devices based on 4Se and 5Se afford PCEs of 15.17% and 15.23%, respectively, with a photoelectric response approaching 1000 nm. More excitingly, the energy loss of the 5Se-based device was as low as 0.477 eV along with almost the smallest non-radiative loss of ~0.15 eV thus far.

Organic solar cells (OSCs), as a very promising technology for next-generation green energy production, have gone through extremely rapid development recently.[1] Among them, non-fullerene acceptors (NFAs) play a crucially important role in boosting the power conversion efficiencies (PCEs) of OSCs, due to their near-infrared absorptions, tunable energy levels, superior intermolecular packings, *etc.*[2–4] To date, single-junction OSCs based on high-efficiency Y-series NFAs[5–8] have exhibited PCEs over 19%.[9] The inner reasons for such an excellent performance should be attributed to the unique but highly favorable three-dimensional (3D) molecular packing network established by Y-series NFAs.[10] Recently, extensive efforts have been made to optimize the structures of Y-series NFAs aiming to reach a record-breaking PCE of OSCs.[11–15] However, dramatic structural modifications will inevitably change the highly desirable 3D molecular packing network of NFAs, which may have an adverse effect on the already efficient charge transport channels. Therefore, the structural modification at atomic levels, like replacing sulfur with selenium, has attracted great attention in order to enhance both the light-harvesting and charge transfer/transport abilities without damaging the superior molecular packings.[16–20]

As is well-known, selenium can be easily polarized with respect to sulfur. Therefore, the better electron cloud delocalization of selenium usually causes relatively larger orbital overlap in π-conjugated systems, resulting in decreased aromaticity and enhanced quinoidal character.[15] Moreover, replacing S with Se could keep the skeleton characteristics of molecules to the maximum, and generate minimal impacts on molecular geometries and further intermolecular packing networks. Bearing these thoughts in mind, a seleno[3,2-*b*]selenophene unit has been synthesized and employed to construct NFAs for the first time (Fig. 1a). Two near-infrared NFAs of **4Se** and **5Se** are constructed by replacing four or all sulfurs in high-efficiency Y-series NFAs with selenium. Consequently, binary devices based on **4Se** and **5Se** afforded PCEs of 15.17% and 15.23%, respectively, with a photoelectric response approaching 1000 nm. More excitingly, the energy loss of the **5Se**-based device was as low as 0.477 eV along with almost the smallest non-radiative loss of ~0.15 eV thus far. By extending Se substitution to the limit in high-efficiency Y-series NFAs, we maximized and further unveiled the effects of selenium on the physico-chemical properties, intermolecular packings and even photovoltaic performance of NFAs.

The synthetic route to 4Se and 5Se is shown in Fig. 1 and the detailed procedures and characterizations are presented in the ESI.† Firstly, 3-bromoselenophene was lithiated and treated with selenium powder and ethyl 2-bromoacetate stepwise to afford compound 2 with a relatively low yield of 24%. Then compound 2 was converted to compound 3 by a Friedel–Crafts reaction catalysed by $AlCl_3$. Furthermore, hydrolysis of compound 3 was conducted under base conditions, followed by an acidification to generate the corresponding acid 4 in a good yield (84%). Finally, the key intermediate of seleno[3,2-*b*]selenophene (5) was yielded by decarboxylation of acid 4 using silver carbonate. Afterwards, through the classic synthesis

[a] *State Key Laboratory and Institute of Elemento-Organic Chemistry, The Centre of Nanoscale Science and Technology and Key Laboratory of Functional Polymer Materials, Renewable Energy Conversion and Storage Center (RECAST), College of Chemistry, Nankai University, Tianjin 300071, China*
[b] *School of Materials Science and Engineering, National Institute for Advanced Materials, Nankai University, Tianjin, 300350, China*

† Electronic supplementary information (ESI) available. See DOI: https://doi.org/10.1039/d3cc02560h

‡ These authors contributed equally to this work.

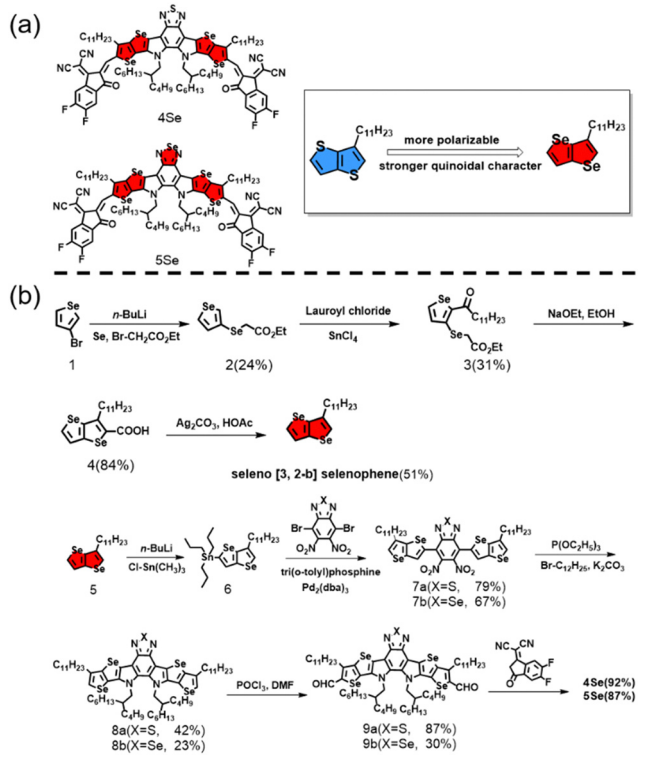

Fig. 1 The chemical structures (a) and synthetic routes (b) of **4Se** and **5Se**.

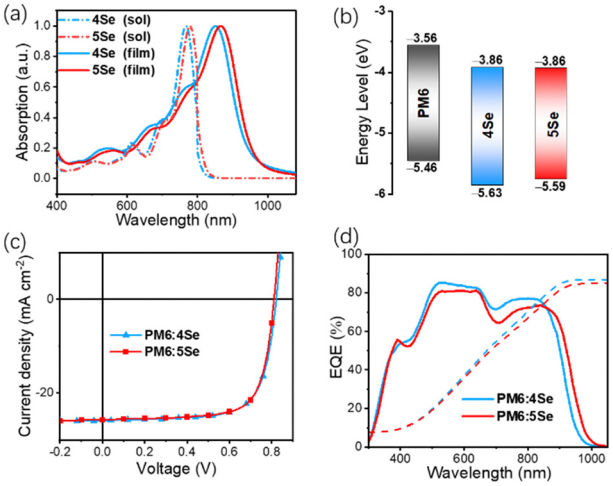

Fig. 2 (a) Normalized absorption spectra of **4Se** and **5Se** in diluted solutions of chloroform and neat films. (b) Energy level diagram of **PM6**, **4Se** and **5Se** derived from electrochemical cyclic voltammetry. (c) Current density–voltage (*J*–*V*) of the optimized devices and (d) EQE curves.

route,[5] including Stille coupling, Cadogan cyclization, Vilsmeier formylation and Knoevenagel condensation reactions, 4Se and 5Se were afforded as blue-black solids. The molecular structures of **4Se**[21] and **5Se** have been fully characterized by analysis of nuclear magnetic resonance (NMR) spectroscopy and high-resolution mass spectroscopy (HRMS) (Fig. S5–S14, ESI†). Note that both **4Se** and **5Se** can be well dissolved in widely used solvents like chloroform and chlorobenzene, being conducive to fabricating OSCs through solution processing.

The light absorption properties of **4Se** and **5Se** in diluted solutions and thin-films were indicated by corresponding UV-vis spectra in Fig. 2a. **4Se** and **5Se** display the maximum absorption wavelengths of 767 and 778 nm in solution. Moreover, an obvious red-shifting of ~90 nm can be observed for **4Se** and **5Se** neat films with absorption peaks located at 852 and 865 nm, respectively, suggesting strong intermolecular interactions.[22] Both **4Se** and **5Se** exhibit strong near-infrared absorption with onsets extending to 945 and 962 nm, indicating an optical bandgap (E_g) of 1.312 and 1.289 eV, respectively. It is worth noting that with more electron-rich selenium atoms on the molecular skeletons of NFAs, an enhanced light harvesting ability, especially in low energy regions, could be achieved, which should be mainly attributed its upshifted highest occupied molecular orbital (HOMO). Therefore, cyclic voltammetry (CV) was further employed to investigate variations of the frontier molecular orbital energy levels of **4Se** and **5Se** (Fig. S2, ESI†) and the derived energy level diagram has been illustrated in Fig. 2b. The specific data of the HOMOs and the lowest unoccupied molecular orbitals (LUMOs) are also listed in Table S1 (ESI†). The HOMO/LUMO energy levels of **4Se** and **5Se** were −5.63/−3.86 eV and −5.59/−3.86 eV, respectively. The significantly upshifted HOMO for **5Se** compared with that of **4Se** should be caused by the more electron-rich character of selenium in **5Se** than sulfur in **4Se**. Furthermore, the smaller energy difference in the HOMO levels between **5Se** and the commonly used polymeric donor **PM6** (as shown in Fig. 2a) is expected to lead to a reduction in energy losses (E_{loss}) of 5Se-based OSCs.[23] Additionally, density functional theory (DFT) calculations were performed to evaluate the effects of more selenium substitution on the molecular geometries and energy levels. The optimized molecular geometries of **4Se** and **5Se** are illustrated in Fig. S1 (ESI†), and both of them show excellent planar conformations. The calculated HOMO/LUMO energy levels for **4Se** and **5Se** were found to be −5.56/−3.58 eV and −5.52/−3.56 eV (Fig. S1, ESI†), which is consistent with the relative energy level alignment obtained from CV curves. Note that the HOMOs for both NFAs are mainly located on the central donors; however, the LUMOs are delocalized along the whole molecular backbones with a relatively larger concentration on electron-deficient terminals. The sufficient overlap of the frontier molecular orbitals is expected to give rise to an efficient intramolecular charge transfer in such A–D–A type NFAs.[12]

To evaluate the photovoltaic performance of **4Se** and **5Se**, conventional OSCs with **PM6** as a polymeric donor were fabricated. Table 1 presents the photovoltaic parameters of the leading OSCs, while Fig. 2c displays the corresponding current density–voltage (*J*–*V*) curves. As shown in Table 1, OSCs based on **PM6:4Se** give rise to an optimal PCE of 15.17% with a V_{OC} of 0.822 V, a J_{SC} of 25.96 mA cm^{-2} and an FF of 71.08%. Meanwhile, **PM6:5Se**-based OSCs exhibited a slightly lower V_{OC} (0.812 V) and a comparable J_{SC} (25.73 mA cm^{-2}) and a larger FF (72.93%), thus rendering a slightly improved PCE of 15.23%. Note that the J_{SC} values obtained by integrating external

Table 1 Photovoltaic performance parameters of OSCs based on **PM6**:**4Se** and **PM6**:**5Se** measured under the illumination of AM 1.5G (100 mW cm^{-2})[a]

Devices	V_{OC} [V]	J_{SC} [mA cm^{-2}]	J_{SC} (EQE_{cal})[b] [mA cm^{-2}]	FF [%]	PCE [%]
PM6:4Se	0.822 (0.819 ± 0.01)	25.96 (25.68 ± 0.30)	25.73	71.08 (70.67 ± 1.04)	15.17 (14.86 ± 0.21)
PM6:5Se	0.812 (0.808 ± 0.01)	25.74 (25.99 ± 0.42)	24.96	72.93 (71.81 ± 1.03)	15.23 (15.09 ± 0.09)

[a] The values in parentheses are average parameters obtained from 10 devices. [b] The J_{SC} (EQE_{cal}) is determined from the integration of the EQEs to the AM1.5G spectrum.

quantum efficiency (EQE) plots (Fig. 2d) agree well with the values derived from *J*–*V* curves, which are limited in 5% error. Although the EQE values for **5Se**-based OSCs are smaller than those of **4Se**-based ones, a comparable integrated J_{SC} can be still achieved due to the enhanced photoelectric response in the NIR region for **5Se**. Moreover, space charge limited current (SCLC) measurements were further carried out to estimate the mobility of the charge carrier in the blended films. As shown in Fig. S3 and Table S4 (ESI†), based on the average results of 10 devices, the hole mobilities for **PM6:4Se** and **PM6:5Se** are 6.09×10^{-4} and 5.99×10^{-4} cm^2 V^{-1} s^{-1}, respectively, and the corresponding electron mobilities are 7.20×10^{-4} and 5.77×10^{-4} cm^2 V^{-1} s^{-1} for **PM6:4Se** and **PM6:5Se** blends, respectively. The comparable but more balanced charge carrier mobilities for **PM6:5Se** blends will be conducive to facilitated charge transport in the resulting OSCs.[24] Surprisingly, although **5Se**-based OSCs afford a slightly smaller V_{OC} than **4Se**-based ones, the energy loss (E_{loss}) of the **5Se**-based OSCs is only 0.477 eV, smaller than that of 0.490 eV for **4Se**-based devices (see analysis below for details).

To understand the effects of all selenium substitution on molecular packing and crystallinity orientation, grazing incidence wide angle X-ray scattering (GIWAXS) was further performed. Efficient vertical charge transport channels between two electrodes were provided by the predominant face-on orientation observed in all samples.[25] When taking a more in-depth observation, we found that **4Se** and **5Se** films possess (010) peaks at 1.69 and 1.67 $Å^{-1}$, corresponding to a π–π stacking distance of 3.71 and 3.75 Å, respectively (Table S2, ESI†). After blending with the **PM6** donor, tighter π–π stacking can be suggested by a decreased π–π stacking distance of 3.64 Å for **PM6:4Se** and 3.68 Å for **PM6:5Se**. The slightly enlarged π–π stacking distance for **5Se**-based films compared to that of **4Se**-based ones should be caused by the larger atomic radius of selenium (103 pm) with respect to sulfur (88 pm). Furthermore, the crystal coherence length (CCL) in the (010) region is 26.67 Å for the **PM6:5Se** blend, which is larger than that of the **PM6:4Se** blend with a CCL of 23.24 Å. The increased CCL for **PM6:5Se** implies a more ordered molecular packing, which will be favorable to suppress charge recombination and reduce E_{loss} in the resulting OSCs (Fig. 3).[17]

As it has been discussed above, **5Se** indeed possesses a narrower optical bandgap than **4Se** (Fig. 2a). However, **5Se**-based OSCs possess only slightly dropped V_{OC} (0.812 eV) with respect to that of 0.822 eV for **4Se**-based ones. Thus, an exciting deduction can be afforded that a smaller E_{loss} for **5Se**-based OSCs may be achieved. Therefore, the detailed

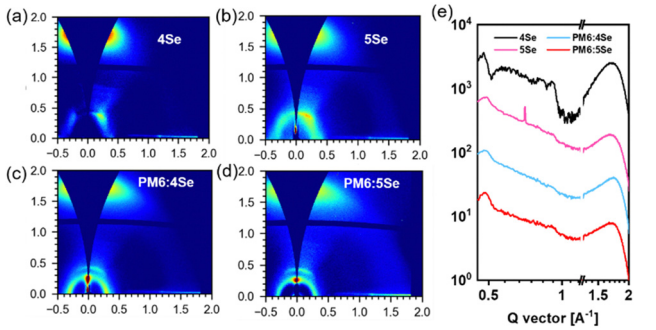

Fig. 3 Two dimensional GIWAXS patterns for the (a) **4Se** blend, (b) **5Se** blend, (c) **PM6**:**4Se** blend and (d) **PM6**:**5Se** blend. (e) Out-of-plane line cuts of the corresponding GIWAXS patterns.

E_{loss} analysis of the OSCs was further conducted. Based on the detailed balance theory,[26] E_{loss} can be divided into three parts, ΔE_1, ΔE_2 and ΔE_3 (see ESI† for the details). ΔE_1 depends on the bandgap, which is 0.256 and 0.254 eV for **PM6:4Se** and **PM6:5Se**-based OSCs, respectively (Table S3, ESI†). Radiative recombination loss below the bandgap is represented by ΔE_2, being 0.067 and 0.073 eV for **PM6:4Se** and **PM6:5Se**-based OSCs, respectively. ΔE_3 is the most important non-radiative energy loss in OSCs. Herein, **PM6:4Se**-based OSCs generate a value of 0.167 eV for ΔE_3, while it has decreased to 0.152 eV for **PM6:5Se**-based OSCs. This is possibly caused by the more ordered intermolecular packing in **5Se**-based films, which can be concluded by the GIWAXS measurements. Moreover, the reduced ΔE_3 of **PM6:5Se**-based OSCs is also confirmed by the higher external electroluminescence quantum efficiencies (EQE_{EL}) in Fig. S4 (ESI†).[27] It is worth noting that the **PM6:5Se**-based OSC concurrently reached an excellent PCE of 15.23% and considerably low ΔE_3 of 0.152 eV, which should be the best OSC with $\Delta E_3 \leq 0.16$ eV to date (Table S5, ESI†).[28–32]

In summary, based on a newly synthesized seleno [3,2-b]selenophene unit, we have extended Se substitution to the limit and constructed two NIR NFAs of **4Se** and **5Se**. Benefitting from the looser outmost electron cloud, easily polarized characteristic and improved quinoidal resonance of selenium with respect to those of sulfur, **5Se** gives rise to an obviously redshifted absorption and more ordered molecular packings compared to **4Se**. As a result, **PM6:4Se** and **PM6:5Se**-based OSCs afforded a relatively high PCE of 15.17% and 15.23%, respectively, with a photoelectric response approaching 1000 nm. More excitingly, the energy loss of the **5Se**-based device was as low as 0.477 eV along with almost the smallest non-radiative loss of ~0.15 eV thus far. By extending Se

substitution to the limit in high-efficiency Y-series NFAs, we maximized and unveiled the effects of selenium on the physicochemical properties, intermolecular packings and even photovoltaic performance of NFAs; meanwhile, this will stimulate further efforts to apply the Se substitution strategy in other efficient NFA systems with the aim of achieving better OSCs.

The authors gratefully acknowledge the financial support from Ministry of Science and Technology of the People's Republic of China (National Key R&D Program of China, 2022YFB4200400, 2019YFA0705900) and National Natural Science Foundation of China (21935007, 52025033, 51873089), Tianjin city (20JCZDJC00740, 22JCQNJC00530), 111 Project (B12015) and Haihe Laboratory of Sustainable Chemical Transformations.

Conflicts of interest

There are no conflicts to declare.

Notes and references

1 Z. Zheng, J. Wang, P. Bi, J. Ren, Y. Wang, Y. Yang, X. Liu, S. Zhang and J. Hou, *Joule*, 2021, **6**, 171–184.
2 G. Yu, J. Gao, J. C. Hummelen, F. Wudl and A. J. Heeger, *Science*, 1995, **270**, 1789–1791.
3 Z. Li, G. He, X. Wan, Y. Liu, J. Zhou, G. Long, Y. Zuo, M. Zhang and Y. Chen, *Adv. Energy Mater.*, 2012, **2**, 74–77.
4 J. S. Wu, S. W. Cheng, Y. J. Cheng and C. S. Hsu, *Chem. Soc. Rev.*, 2015, **44**, 1113–1154.
5 J. Yuan, Y. Zhang, L. Zhou, G. Zhang, H.-L. Yip, T.-K. Lau, X. Lu, C. Zhu, H. Peng, P. A. Johnson, M. Leclerc, Y. Cao, J. Ulanski, Y. Li and Y. Zou, *Joule*, 2019, **3**, 1140–1151.
6 Y. Cui, H. Yao, J. Zhang, K. Xian, T. Zhang, L. Hong, Y. Wang, Y. Xu, K. Ma, C. An, C. He, Z. Wei, F. Gao and J. Hou, *Adv. Mater.*, 2020, **32**, e1908205.
7 C. Li, J. Zhou, J. Song, J. Xu, H. Zhang, X. Zhang, J. Guo, L. Zhu, D. Wei, G. Han, J. Min, Y. Zhang, Z. Xie, Y. Yi, H. Yan, F. Gao, F. Liu and Y. Sun, *Nat. Energy*, 2021, **6**, 605–613.
8 H. Chen, Y. Zou, H. Liang, T. He, X. Xu, Y. Zhang, Z. Ma, J. Wang, M. Zhang, Q. Li, C. Li, G. Long, X. Wan, Z. Yao and Y. Chen, *Sci. China: Chem.*, 2022, **65**, 1362–1373.
9 T. Chen, S. Li, Y. Li, Z. Chen, H. Wu, Y. Lin, Y. Gao, M. Wang, G. Ding, J. Min, Z. Ma, H. Zhu, L. Zuo and H. Chen, *Adv. Mater.*, 2023, e2300400, DOI: 10.1002/adma.202300400.
10 W. Zhu, A. P. Spencer, S. Mukherjee, J. M. Alzola, V. K. Sangwan, S. H. Amsterdam, S. M. Swick, L. O. Jones, M. C. Heiber, A. A. Herzing, G. Li, C. L. Stern, D. M. DeLongchamp, K. L. Kohlstedt, M. C. Hersam, G. C. Schatz, M. R. Wasielewski, L. X. Chen, A. Facchetti and T. J. Marks, *J. Am. Chem. Soc.*, 2020, **142**, 14532–14547.
11 Y. Shi, Y. Chang, K. Lu, Z. Chen, J. Zhang, Y. Yan, D. Qiu, Y. Liu, M. A. Adil, W. Ma, X. Hao, L. Zhu and Z. Wei, *Nat. Commun.*, 2022, **13**, 3256.
12 Y. Zou, H. Chen, X. Bi, X. Xu, H. Wang, M. Lin, Z. Ma, M. Zhang, C. Li, X. Wan, G. Long, Y. Zhaoyang and Y. Chen, *Energy Environ. Sci.*, 2022, **15**, 3519–3533.
13 H. Meng, C. Liao, M. Deng, X. Xu, L. Yu and Q. Peng, *Angew. Chem., Int. Ed.*, 2021, **60**, 22554–22561.
14 F. Liu, L. Zhou, W. Liu, Z. Zhou, Q. Yue, W. Zheng, R. Sun, W. Liu, S. Xu, H. Fan, L. Feng, Y. Yi, W. Zhang and X. Zhu, *Adv. Mater.*, 2021, **33**, e2100830.
15 B. Fan, F. Lin, X. Wu, Z. Zhu and A. K. Jen, *Acc. Chem. Res.*, 2021, **54**, 3906–3916.
16 F. Lin, K. Jiang, W. Kaminsky, Z. Zhu and A. K. Jen, *J. Am. Chem. Soc.*, 2020, **142**, 15246–15251.
17 Z. Zhang, Y. Li, G. Cai, Y. Zhang, X. Lu and Y. Lin, *J. Am. Chem. Soc.*, 2020, **142**, 18741–18745.
18 F. Huang, Z. Li, G. Song, C. Jiang, Y. Yang, J. Wang, X. Wan, C. Li, Z. Yao and Y. Chen, *Adv. Funct. Mater.*, 2022, **33**, 2211140.
19 J. Zhang, S. Luo, H. Zhao, X. Xu, X. Zou, A. Shang, J. Liang, F. Bai, Y. Chen, K. S. Wong, Z. Ma, W. Ma, H. Hu, Y. Chen and H. Yan, *Angew. Chem., Int. Ed.*, 2022, **61**, e202206930.
20 G. Chai, J. Zhang, M. Pan, Z. Wang, J. Yu, J. Liang, H. Yu, Y. Chen, A. Shang, X. Liu, F. Bai, R. Ma, Y. Chang, S. Luo, A. Zeng, H. Zhou, K. Chen, F. Gao, H. Ade and H. Yan, *ACS Energy Lett.*, 2020, **5**, 3415–3425.
21 L. Meng, H. Liang, G. Song, M. Li, Y. Huang, C. Jiang, K. Zhang, F. Huang, Z. Yao, C. Li, X. Wan and Y. Chen, *Sci. China: Chem.*, 2023, **66**, 808–815.
22 R. Steyrleuthner, M. Schubert, I. Howard, B. Klaumunzer, K. Schilling, Z. Chen, P. Saalfrank, F. Laquai, A. Facchetti and D. Neher, *J. Am. Chem. Soc.*, 2012, **134**, 18303–18317.
23 Y. Xu, H. Yao, L. Ma, J. Wang and J. Hou, *Rep. Prog. Phys.*, 2020, **83**, 082601.
24 M. M. Mandoc, L. J. A. Koster and P. W. M. Blom, *Appl. Phys. Lett.*, 2007, **90**, 133504.
25 W. Gao, F. Qi, Z. Peng, F. R. Lin, K. Jiang, C. Zhong, W. Kaminsky, Z. Guan, C. S. Lee, T. J. Marks, H. Ade and A. K. Jen, *Adv. Mater.*, 2022, **34**, e2202089.
26 U. Rau, B. Blank, T. C. M. Muller and T. Kirchartz, *Phys. Rev. Appl.*, 2017, **7**, 044016.
27 U. Rau, *Phys. Rev. B: Condens. Matter Mater. Phys.*, 2007, **76**, 085303.
28 L. Perdigon-Toro, H. Zhang, A. Markina, J. Yuan, S. M. Hosseini, C. M. Wolff, G. Zuo, M. Stolterfoht, Y. Zou, F. Gao, D. Andrienko, S. Shoaee and D. Neher, *Adv. Mater.*, 2020, **32**, e1906763.
29 R. Wang, Y. Yao, C. Zhang, Y. Zhang, H. Bin, L. Xue, Z. G. Zhang, X. Xie, H. Ma, X. Wang, Y. Li and M. Xiao, *Nat. Commun.*, 2019, **10**, 398.
30 Y. Xu, Y. Cui, H. Yao, T. Zhang, J. Zhang, L. Ma, J. Wang, Z. Wei and J. Hou, *Adv. Mater.*, 2021, **33**, e2101090.
31 T. Dai, A. Tang, Z. He, M. Du, P. Lei, Z. Wang, Q. Zeng, Y. Wang, S. Lu, Y. Zhong and E. Zhou, *Energy Environ. Sci.*, 2023, **16**, 2199–2211.
32 M. Xie, Y. Shi, H. Zhang, J. Pan, J. Zhang, Z. Wei and K. Lu, *Chem. Commun.*, 2022, **58**, 4877–4880.

